PAPER

Check for updates

Soft particles in an electric field – a zero average contrast study

Sofi Nöjd,[a] Christopher Hirst, [iD] [a] Marc Obiols-Rabasa,[a] Julien Schmitt, [iD] [a] Aurel Radulescu,[b] Priti S. Mohanty[ac] and Peter Schurtenberger [iD] *[ad]

We report on the structural properties of ionic microgel particles subjected to alternating electric fields, using small-angle neutron scattering. The experiments were performed under so-called zero average contrast conditions, which cancel the structure factor contribution to the scattered intensity, allowing us to obtain direct information on the single particle size and structure as particles align in field-induced strings. Our results reveal only a marginal compression of the particles as they align in strings, and indicate considerable particle overlap at higher field strengths. These findings provide further insight into the origins of the previously reported unusual path dependent field-induced crystal-crystal transition found for these systems (P. S. Mohanty *et al.*, *Phys. Rev. X*, 2015, **5**, 011030).

In the area of electrorheological fluids, the concept of responsive dielectric particles has been used for a long time to tune flow properties of colloidal dispersions. In such systems, the bulk viscosity can be significantly altered by an applied electric field, which has made them particularly interesting for industrial applications such as fast hydraulics and brake systems.[1] In the colloid community, the use of direct or alternating electric fields has shown to be an exciting tool to control and direct self-assembly, and a variety of equilibrium structures have been reported for hard sphere systems as a function of dipolar strength and particle charge.[2–5] These field-induced structures have also been reproduced by computer simulations.[6,7] To extend this work, the use of soft colloids such as thermoresponsive microgels has shown to be an intriguing alternative to hard sphere systems due to their more versatile interaction potential. The inhomogeneous radial density profile of microgel particles with a more loosely crosslinked outer shell makes it possible to pack them to extremely high effective volume fractions, resulting in a center-to-center distance, a_s, that can be smaller than the particle diameter in the dilute regime.[8] Ionic microgels represent a particularly interesting class of soft particles, where the resulting interaction potential contains additional contributions from the present interior and surface charges.[9] Due to the interplay between internal and external osmotic pressures and the

sensitivity of the long dangling chains to the bulk ionic strength, ionic microgels have shown a complex response to their environment and variations in particle concentration, pH, ionic strength and temperature.[10,11]

Previous work using ionic microgel particles have demonstrated their capability to form field-induced structures when subjected to alternating external fields.[12–15] These particles possess a strongly enhanced polarizability, caused by the combination of a large fraction of internal and external mobile counterions and the polarizability of the polymer network.[16] This makes them ideal model systems to investigate the formation of string fluids under the influence of an electric field, which then assemble into crystal structures as the dipolar strength (or field strength) is further increased.[17] Surprisingly, the resulting field-induced crystal–crystal transitions were found to be path-dependent. Not only did the interpenetrable and compressible nature of the particles result in the existence of long-lived metastable crystal structures, but these phase transitions were found to follow different paths with a field-induced intermediate melting, nucleation and growth in one direction, and a diffusionless martensitic transformation after the field was turned off.[14]

While there is no quantitative understanding of the origins of this path dependence and the existence of long-lived metastable states, the existing data indicates that the intrachain particle overlap in the strings is mainly responsible for stabilizing the metastable structures.[8,14] It has thus become clear that a better understanding of these observations will require additional information about the response of the individual particles to the field and the subsequent string formation. This would allow obtaining a more quantitative knowledge of the resulting interaction potential in the absence and presence of the field, and the subsequent calculation of the energy of the various equilibrium

[a] *Division of Physical Chemistry, Department of Chemistry, Lund University, SE-22100 Lund, Sweden*

[b] *Jülich Centre for Neutron Science, Heinz Maier-Leibnitz Zentrum, Garching, Germany*

[c] *School of Chemical Technology, Kaligan Institute of Industrial Technology (KIIT), Bhubaneswar, India*

[d] *Lund Institute of advanced Neutron and X-ray Science (LINXS), Lund University, Lund, Sweden. E-mail: Peter.Schurtenberger@fkem1.lu.se*

and non-equilibrium structures. Since the dipolar contribution to the potential is highly affected by the size and shape of individual particles, quantitative information on possible deformations of particles as they form strings is thus needed. In the present work we report on the use of small-angle neutron scattering experiments under zero average contrast conditions to study changes in the internal structure of single particles as they respond to an alternating electric field.

1 Material and methods

Hydrogenated, Hm, and deuterated, Dm, ionic poly(*N*-isopropyl-(acrylamide)), pNIPAM, particles were synthesised *via* precipitation polymerisation in the presence of the co-monomer acrylic acid, AA, and a surfactant[18] to control the internal charge and the final size of the particles, respectively, as described elsewhere.[11] During the synthesis *N*-isopropyl(acrylamide), NIPAM, was used as the main monomer and *N,N*-methylenebisacrylamide, BIS, was used as a crosslinker. The exact amount of the used chemicals can be seen in Table 1. The particle suspensions were cleaned by repeated centrifugation and re-dispersion steps and freeze-dried in order to prepare samples with well-controlled weight concentration. All samples were kept on ion-exchanging resins (Amberlite IRN 150, Fluka) to ensure a constant low background ionic strength. The resins were changed at least 3 times prior to measurements in intervals of 2–3 days and left on a shaker to deionise.

The two sets of particles were first characterized by means of dynamic and static light scattering using a modulated 3D light scattering setup (LS Instruments, Switzerland) at a laser wavelength of 660 nm. Here the pH of the solutions was lowered to 3.2 by the addition of HCl in order to suppress screened Coulomb interactions between particles and prevent a concentration-induced deswelling of the particles that was previously reported in the literature.[10] The hydrodynamic radii were extracted using a first order cumulant analysis averaged over an angular range of $45° \leq \theta \leq 65°$ with a step size of $10°$. The molecular weights of the two sets of particles were found to be $M_{w,Hm} = 2.1 \times 10^9$ g mol^{-1} and $M_{w,Dm} = 2.9 \times 10^9$ g mol^{-1}, respectively, based on a Zimm plot analysis. Conductometric titrations showed that the two sets of particles had an equivalent number of charges. For the subsequent measurements of their field-induced behavior, particles were then deionised as described above. To locate the fluid-string transition, experiments were performed using a confocal laser scanning microscope, CLSM (Leica DMI6000) with a SP5 tandem scanner in the bright field mode (Leica, Germany). The measurements were conducted at 20 °C using a $100\times$ objective with a numerical

aperture of 1.4. Small-angle neutron scattering, SANS, experiments were conducted on the KWS-2 beam-line in Garching, Germany, using a sample-to-detector and collimation distance of 20 m, respectively. A neutron beam with a wavelength of 10 Å and a wavelength spread of 20% was used, giving a *q*-range of $1.49 \times 10^{-3} \leq q \leq 1.96 \times 10^{-2}$ Å^{-1}. Form factors in the absence of field were obtained using a defining aperture of 6×8 mm. Form factor measurements in the presence of field were performed using a defining aperture of 0.8×18 mm, placed on the custom-made sample stage.

2 Results

The change in hydrodynamic radius as a function of increasing temperature for Hm and Dm can be seen in Fig. 1A. For Hm the characteristic drop in size around 33 °C can be observed, whereas for Dm the transition temperature is shifted to slightly higher temperatures due to isotope effects. Since the titratable co-monomer has a pK_a of around 4.2, the pH was here set to 3.2, restraining the osmotic swelling of particles. The linear deswelling behavior normally observed for ionic pNIPAM microgels in the studied temperature range is thus suppressed.[19] To estimate the degree of swelling of the two particles, their swelling ratio, $(R_{h,15°C}/R_{h,45°C})^3$, was calculated and found to be 5.9 and 6.6 for Hm and Dm, respectively. The normalised swelling curve in Fig. 1B confirms that the two particles have a similar temperature-induced deswelling behavior for an extended temperature range below the collapse transition.

CLSM was used to directly determine the field strength for the onset of the fluid-string transition for the fully deionised suspensions. These experiments were performed in bright field mode, since the particles were not fluorescently labeled. Here an electrode with a gap width of 0.334 mm was made by gold/palladium sputtering of a microscope cover slip. The characteristic slowing down of the particle motion and the formation of particle strings in response to the field was observed for a 1 wt% microgel mixture around 100 V mm^{-1}. Due to the use of bright field mode, at low field strengths the image quality was reduced. At higher field strengths, where the strings are getting stiffer and start to assemble into bundles, the image quality was improved as demonstrated in Fig. 2, for a field strength of 150 V mm^{-1}.
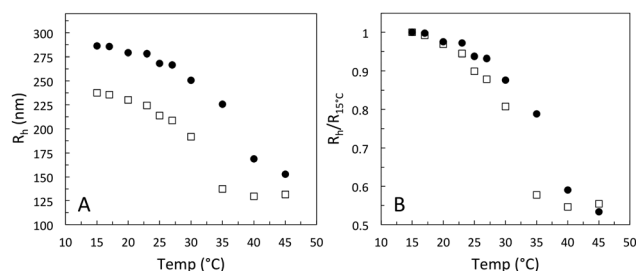
Table 1 Amount of added chemicals in the particle synthesis. The particle name Dm corresponds to the use of a deuterated monomer and acrylic acid. The total reaction volume was 100 ml

Particle name	NIPAM (g)	BIS (g)	AA (g)
Hm	1.43	0.112	0.081
Dm	1.52	0.178	0.082

Fig. 1 (A) Swelling curves as a function of increasing temperature for Hm, open black squares, and Dm, black circles. The solution pH is set to 3.2 to eliminate concentration induced deswelling effects. (B) The same data as presented in A but normalised by $R_{h,15°C}$.
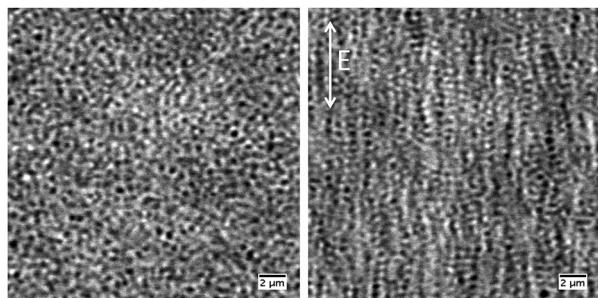
Fig. 2 Left: Image of a particle suspension of 1 wt% in the absence of field taken by CLSM. Right: Image of a particle suspension of 1 wt% in the presence of field (150 V mm^{-1}) taken by CLSM. The applied field direction is illustrated by the white arrow.

Despite the increased image quality, the limited resolution of confocal microscopy does not allow us to obtain detailed information on single particle properties as they respond to the applied field. This can, however, be achieved by performing SANS measurements under so-called zero average contrast, ZAC, conditions.[8,11,20] ZAC experiments rely on the use of a 50–50 mix (by numbers) of otherwise identical deuterated and hydrogenated particles in a solvent with a scattering length density ρ_s that corresponds to the average of the values for the hydrogenated (ρ_{Hm}) and deuterated (ρ_{Dm}) particles. The differential cross-section, $d\sigma(q)/d\Omega$, can be divided into the self (I) and distinct (II) part of the partial structure factor as

$$\frac{d\sigma}{d\Omega} \propto \Delta\rho_{ZAC}^2 \left(S_{Hm}^{I} + S_{Dm}^{I} + S_{HmHm}^{II} + S_{DmDm}^{II} - 2S_{HmDm}^{II} \right) \quad (1)$$

where the scattering contrast is given by $\Delta\rho_{ZAC} = \Delta\rho_{Dm} = -\Delta\rho_{Hm}$. If the particle properties are the same and the interactions between Hm and Dm are assumed to be identical, eqn (1) reduces to

$$\frac{d\sigma}{d\Omega} \propto \Delta\rho_{ZAC}^2 2S_{ZAC}^{I} \propto n_p \Delta\rho_{ZAC}^2 P(q) \quad (2)$$

where n_p is the number density. Measurements were performed by first conducting a contrast variation study of the individual set of particles at low concentrations and with the same number density, as can be seen in Fig. 3. To cancel the contributions from the structure factor caused by screened
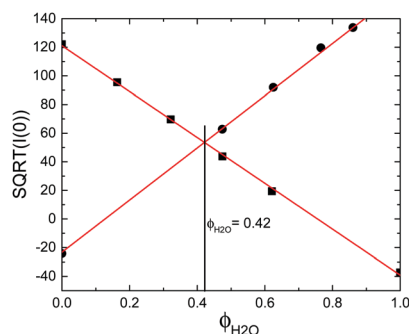
Coulomb interactions, 5 mM of KCl was added to all samples. The ratio H_2O/D_2O was varied for a fixed number density of Hm and Dm particles, respectively. The solvent composition in which the two sets of particles equally contribute to the contrast was found to be 42 v% H_2O and 58 v% D_2O. Equal number density mixtures of Hm and Dm particles were thereafter prepared in the ZAC solvent, without the addition of salt or acid, and left to deionize against ion exchange resins.

In order to conduct SANS experiments in the presence of a alternating electric field, custom-made electrodes were designed, as can be seen in Fig. 4A and B. Here, glass rods coated with gold were used as electrodes with a separation distance of 1 mm between the electrodes. The separation distance was set to 1 mm to maximize the scattering volume and hence the scattered intensity. Applying high field strengths in aqueous solutions results in detectable local heating, which has dramatic consequences on the size of microgel particles. To overcome this issue, a custom-made temperature-controlling sample stage was designed, as shown in Fig. 4C. Before the field experiments were conducted, a calibration curve was obtained for each concentration and field strength used. This was achieved by inserting a small external temperature probe between the two electrodes to accurately record the change in temperature as a function of increasing field strength and concentration. The temperature of the Peltier-controlled sample stage was adjusted accordingly to keep a constant temperature of 20 °C inside the sample at all field strengths.

For comparison, a concentration series was measured, in the ZAC solvent, in the absence of field, using standard sample cells and instrument configurations. The obtained scattering curves are shown in Fig. 5A. All samples investigated in this study were in the fluid regime as determined by CLSM. The obtained form factors were analysed with the fuzzy sphere model, which is generally used to describe the varying radial density distribution in microgels, and the resulting fits are illustrated as solid lines in Fig. 5A.[21] In the first analysis of the data, the shell thickness was left as a free parameter and seen to vary marginally, around 5 nm. In the final analysis the shell thickness, 40 nm, and the polydispersity, 12%, were kept constant. The polydispersity was calculated based on the size
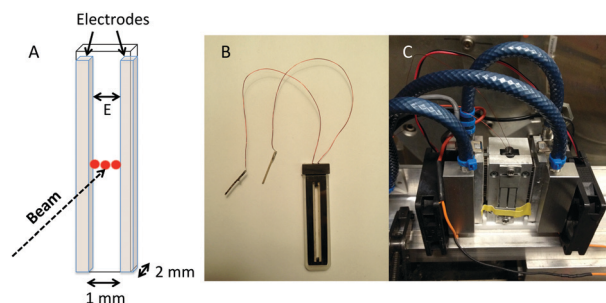

Fig. 3 Contrast variation experiments performed for Hm, black squares, and Dm, black circles, as a function of solvent composition. The structure peak was cancelled in all samples by addition of 5 mM KCl. The solid lines are linear fits to the data.

Fig. 4 (A) Schematic illustration of the electrode used, inserted in a 2 mm path length quartz cuvette. (B) The custom-made electrode used, where two glass rods coated with gold acts as conducting electrodes. (C) Photo of the Peltier-controlled sample stage used during the SANS measurements under electric field.
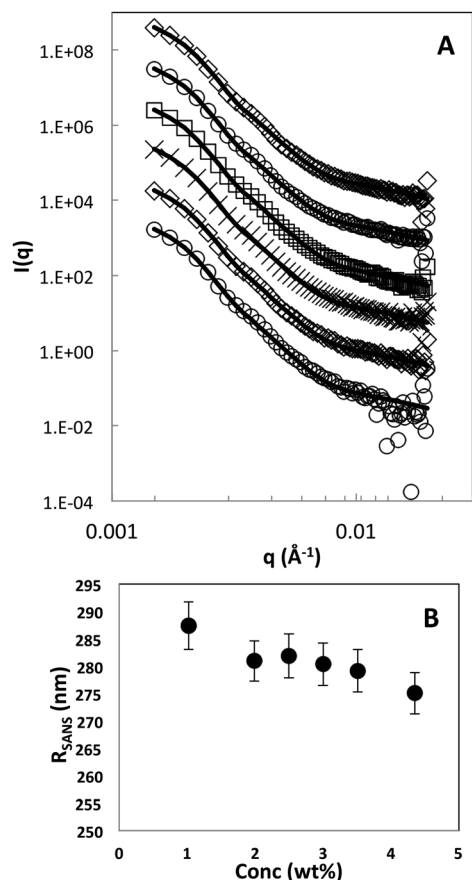
Fig. 5 (A) Scattering curves obtained in the absence of field. Particle concentration is ranging from 1–4 wt%, bottom to top. Solid lines are fits to the data using the fuzzy sphere model. The curves are offset along the ordinate for clarity. (B) The change in particle size, R_{SANS}, as a function of increasing concentration, in the absence of field.

difference between Hm and Dm particles and an intrinsic polydispersity for each batch. The overall particle size, R_{SANS}, as a function of increasing particle concentration is shown in Fig. 5B. The particle size is seen to only decrease by less than 5% in the investigated concentration regime. The small observed deswelling is due to the decreased difference in internal and external osmotic pressure as the particle concentration, and more importantly, the free counter-ion concentration, is increased. The Hm and Dm particles have a similar internal charge as determined from the titration study, and should thus show a similar osmotic deswelling behavior. This has previously also been reported in the literature for a similar system as the one used in this study.[11] However, ionic microgels have shown to possess two deswelling regimes. At low concentrations in the fluid regime, the deswelling can primarily be attributed by osmotic deswelling, whereas in the over-packed state, where the effect of particle charge is minor, it is attributed to elastic compression of the particle shell upon overlap. The latter would give rise to a more significant decrease in the shell thickness due to the compression of overlapping shells, and hence is not present here for the chosen conditions but would only show up at even higher concentrations.

In a next step we then investigated the response of the particle size and shape to an external electric field. In Fig. 6A, scattering data obtained from a field experiment for a microgel concentration of 2.5 wt% are shown. The absence of the structure factor contribution indicates that no segregation of Hm or Dm particles takes place as the field is turned on, and confirms that the ZAC approach works also in the presence of a field that results in string formation. The data is well reproduced by the fuzzy sphere model at all field strengths investigated. From the residual plot shown in Fig. 6B it is evident that no systematic deviation is found as a function of increasing field strength. This clearly demonstrates the absence of a measurable deformation of particles in the strings as the field strength is significantly increased. Moreover, no sign of an anisotropic deformation was observed when analyzing the scattering data along the different sectors of the detector, *i.e.*, horizontal and perpendicular to the field direction.

The results from the ZAC measurements at different concentrations and field strengths are summarized in Fig. 7. The data is shown as the overall particle radius R_{SANS} normalized by the particle radius measured in the absence of a field, R_0. In the presence of the field, only a small change in size was observed
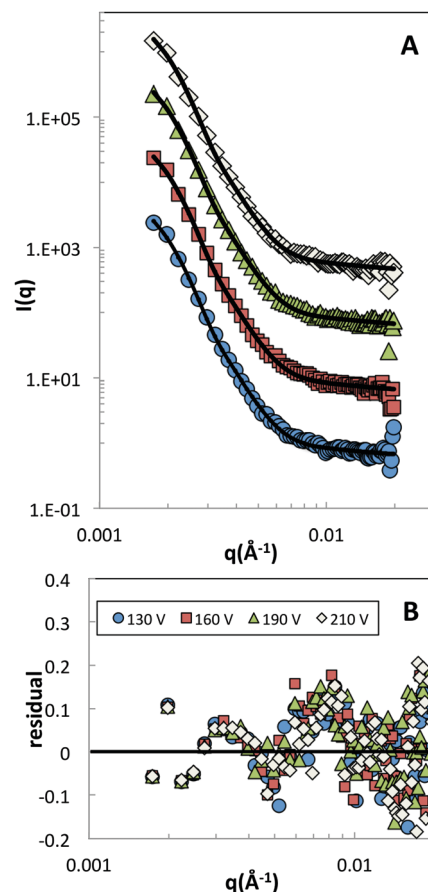

Fig. 6 (A) Scattering curves obtained in the presence of field, 130–210 V mm^{-1}, bottom to top, at a sample concentration of 2.5 wt%. Solid lines are fits to the data using the fuzzy sphere model. The curves are offset along the ordinate for clarity. (B) Residual plot obtained from the fits in (A).
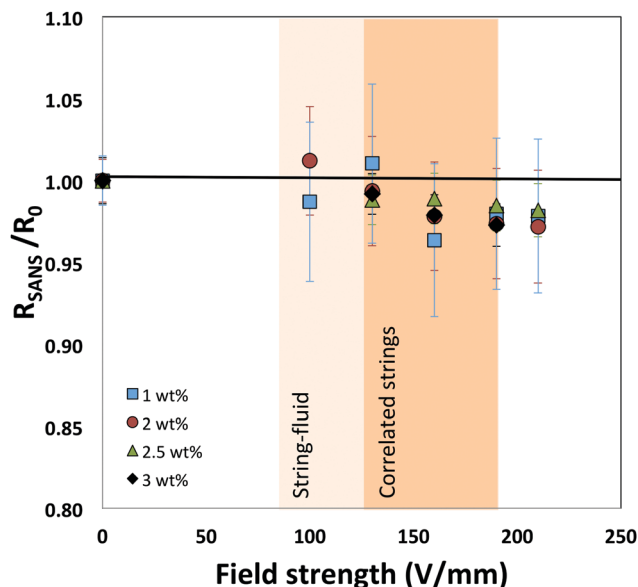
Fig. 7 The change in particle size R_{SANS} as a function of increasing field strength. The data is normalized with the size obtained at zero volt, R_0. The onset of the fluid–sting transition, coloured regions, was determined by direct observations using CLSM.

above a threshold field strength value of around 125 V mm^{-1} for the investigated concentrations. At this field strength CLSM measurements clearly show the formation of strongly correlated strings. Moreover, the center-to-center distance between particles in strings has shown to decrease considerably below the diameter of the particles to values of $a_s/\sigma_0 \approx 0.8$, where a_s is the average center–center distance between particles and σ_0 the diameter of the unperturbed particle, reflecting the resulting balance between the attractive dipolar force and the intrinsic soft repulsive potential at particle overlap.[12,13] Our results thus clearly demonstrate that this strongly reduced interparticle distance between particles in strings is not due to a particle compression and deformation. Instead, the small decrease in particle size of a few percent only, which should be compared with the previously determined values of $a_s/\sigma_0 \approx 0.8$ in the strings, clearly indicates that particles must have a considerable degree of interpenetration along the string direction.

3 Conclusions

By using a combination of scattering and microscopy techniques we have shown that ionic microgels subjected to alternating electric fields decrease their size only marginally when undergoing a transition from individual particles to strongly correlated particle strings. While this could also be caused by the increase in local density when particles form strings, the osmotic deswelling was found to be very small in the investigated concentration range. We thus believe that this weak field-induced deswelling behavior in the investigated field strength regime is primarily due to elastic compression as particle shells start to overlap along the chains. This marginal decrease of the particle radius of 2–3% only has to be compared to the considerable decrease of the

interparticle distance in the chains upon a field-induced string formation.[12,13] This clearly indicates a considerable interpenetration of the outer loosely crosslinked particle shells and dangling ends. Such strong particle interpenetration has previously been observed already for neutral microgels at densities above random close packing.[8] There a simple dissolution experiment using macroscopic droplets of microgels at different densities injected into a large solvent volume had shown that the presence of strong interparticle interpenetration resulted in extremely slow dissolution kinetics for the injected droplets, and indicated that the presence of chain entanglements from the interpenetrated dangling ends introduced an effective attraction between particles and resulted in very long-lived metastable states. We believe that the same phenomenon is also at the origin of the previously discovered existence of long-lived metastable crystalline states in field-induced crystalline structures of strongly correlated particle strings after the field has been turned of, where the field induced body-centered tetragonal (BCT) structure did not relaxed to the ground state face-centered cubic (FCC) crystal, but transformed to a metastable body-centered orthorhombic (BCO) phase.[14] This means that strings that form the BCT crystal structure do not dissolve after the field has been turned of, which would be required to form the FCC structure. Instead, their 3D arrangement slightly relaxes, resulting in a BCO structure, but they remain intact, presumably stabilized by the chain entanglements present in the interpenetrating regions of the microgels in the strings. It is clear that while our experiments provide experimental evidence for such a scenario, additional experiments with microgels that differ in shell thickness and length profile for the dangling ends would be highly interesting as this would allow to unambiguously demonstrate the origin of the unusual field-induced crystal-crystal transition scenarios found for these particles.

Conflicts of interest

There are no conflicts to declare.

Acknowledgements

References

1 M. Parthasarathy and D. J. Klingenberg, *J. Chem. Phys.*, 1996, **17**, 57.
2 U. Dassanayake, S. Fraden and A. van Blaaderen, *J. Chem. Phys.*, 2000, **112**, 3851.

3 A. Yethiraj and A. van Blaaderen, *Int. J. Mod. Phys. B*, 2002, **16**, 2328.

4 A. Yethiraj and A. van Blaaderen, *Nature*, 2003, **421**, 513.

5 A. Yethiraj, A. Wouterse, B. Groh and A. van Blaaderen, *Phys. Rev. Lett.*, 2004, **92**, 058301.

6 A.-P. Hynninen and M. Dijkstra, *Phys. Rev. A: At., Mol., Opt. Phys.*, 2005, **72**, 051402.

7 A.-P. Hynninen and M. Dijkstra, *Phys. Rev. Lett.*, 2005, **94**, 138303.

8 P. S. Mohanty, S. Nöjd, K. van Gruijthuijsen, J. J. Crassous, M. Obiols-Rabasa, R. Schweins, A. Stradner and P. Schurtenberger, *Sci. Rep.*, 2017, **7**, 1487.

9 J. Riest, P. Mohanty, P. Schurtenberger and C. N. Likos, *Z. Phys. Chem.*, 2012, **226**, 711.

10 P. Holmqvist, P. S. Mohanty, G. Nägele, P. Schurtenberger and M. Heinen, *Phys. Rev. Lett.*, 2012, **109**, 048302.

11 S. Nöjd, P. Holmqvist, N. Boon, M. Obiols-Rabasa, P. S. Mohanty, R. Schweins and P. Schurtenberger, *Soft Matter*, 2018, **14**, 4150.

12 P. S. Mohanty, A. Yethiraj and P. Schurtenberger, *Soft Matter*, 2012, **8**, 10819.

13 S. Nöjd, P. S. Mohanty, P. Bagheri, A. Yethiraj and P. Schurtenberger, *Soft Matter*, 2013, **9**, 9199.

14 P. S. Mohanty, P. Bagheri, S. Nöjd, A. Yethiraj and P. Schurtenberger, *Phys. Rev. X*, 2015, **5**, 011030.

15 K. Jathavedan, S. K. Bhat and P. S. Mohanty, *J. Colloid Interface Sci.*, 2019, **544**, 88.

16 P. S. Mohanty, S. Nöjd, M. Bergman, G. Nägele, S. Arrese-Igor, A. Alegria, R. Roa, P. Schurtenberger and J. Dhont, *Soft Matter*, 2016, **12**, 9705.

17 T. Colla, P. S. Mohanty, S. Nöjd, E. Bialik, A. Riede, P. Schurtenberger and C. N. Likos, *ACS Nano*, 2018, **12**, 4321.

18 X. Wu, R. H. Pelton, A. E. Hamielec, D. R. Woods and W. McPhee, *Colloid Polym. Sci.*, 1994, **272**, 467.

19 K. Kratz, T. Hellweg and W. Eimer, *Colloids Surf., A*, 2000, **170**, 137.

20 L. Willner, O. Jucknischke, D. Richter, J. Roovers, L.-L. Zhou, P. M. Toporowski, L. J. Fetters, J. S. Huang, M. Y. Lin and N. Hadjichristidis, *Macromolecules*, 1994, **27**, 3821.

21 M. Stieger, W. Richtering, J. S. Pedersen and P. Lindner, *J. Chem. Phys.*, 2004, **120**, 6197.